AIP Advances

Refractive indices of MBE-grown $Al_xGa_{(1-x)}As$ ternary alloys in the transparent wavelength region

Cite as: AIP Advances **11**, 025327 (2021); https://doi.org/10.1063/5.0039631
Submitted: 04 December 2020 • Accepted: 25 January 2021 • Published Online: 18 February 2021

Konstantinos Papatryfonos, Todora Angelova, Antoine Brimont, et al.

Refractive indices of MBE-grown $Al_xGa_{(1-x)}As$ ternary alloys in the transparent wavelength region

Cite as: AIP Advances 11, 025327 (2021); doi: 10.1063/5.0039631
Submitted: 4 December 2020 • Accepted: 25 January 2021 •
Published Online: 18 February 2021

Konstantinos Papatryfonos,[1,a),b)] Todora Angelova,[2] Antoine Brimont,[2] Barry Reid,[3] Stefan Guldin,[3] Peter Raymond Smith,[1] Mingchu Tang,[1] Keshuang Li,[1] Alwyn J. Seeds,[1] Huiyun Liu,[1] and David R. Selviah[1,a)]

AFFILIATIONS

[1]Department of Electronic and Electrical Engineering, University College London, UCL, Torrington Place, London WC1E 7JE, United Kingdom

[2]Valencia Nanophotonics Technology Center, Universitat Politècnica de València, Camino de Vera, s/n 46022, Spain

[3]Department of Chemical Engineering, University College London, UCL, Torrington Place, London WC1E 7JE, United Kingdom

[a)]**Authors to whom correspondence should be addressed:** k.papatryfonos@ucl.ac.uk, kpapatry@mit.edu; or d.selviah@ucl.ac.uk
[b)]**Current address:** Department of Mathematics, Massachusetts Institute of Technology, Cambridge, Massachusetts 02139, USA.

ABSTRACT

A series of $Al_xGa_{(1-x)}As$ ternary alloys were grown by molecular beam epitaxy (MBE) at the technologically relevant composition range, $x < 0.45$, and characterized using spectroscopic ellipsometry to provide accurate refractive index values in the wavelength region below the bandgap. Particular attention is given to O-band and C-band telecommunication wavelengths around 1.3 μm and 1.55 μm, as well as at 825 nm. MBE gave a very high accuracy for grown layer thicknesses, and the alloys' precise compositions and bandgap values were confirmed using high-resolution x-ray diffraction and photoluminescence, to improve the refractive index model fitting accuracy. This work is the first systematic study for MBE-grown $Al_xGa_{(1-x)}As$ across a wide spectral range. In addition, we employed a very rigorous measurement-fitting procedure, which we present in detail.

I. INTRODUCTION AND LITERATURE ANALYSIS

Precision optical refractive index measurements are important in a wide variety of applications from microlens design[1,2] to optical fiber design,[3,4] especially in the semiconductor industry. The increasingly high performance and modeling and fabrication complexity now required of waveguide-based devices has renewed the interest in extremely accurate refractive index measurements of widely used materials. Recent advances in molecular beam epitaxy (MBE) material growth and in spectroscopic ellipsometry (SE), including both hardware and software developments, now enable this challenge to be addressed with a higher precision than in earlier reported research.

Semiconductor $Al_xGa_{(1-x)}As$ ternary alloys are of high technological relevance, being part of the device epitaxial structure in lasers,[5,6] single photon sources,[7] wavelength division multiplexing (WDM) components,[8] and solar cells.[9] While being virtually lattice-matched to their GaAs substrates over the entire composition range, they have a higher bandgap, which varies continuously with x, and a lower refractive index than GaAs, thus providing a wealth of possibilities for optical waveguides and laser heterostructure design. This unique set of properties makes it easy to enhance the device performance through wide-range bandgap engineering, while keeping an ultra-low dislocation density. In order to fully benefit from these opportunities, we need to develop accurate models of the desired optoelectronic devices using such alloys, and for that, a very precise knowledge of the refractive indices is required.

Due to its great importance, a number of models and experimental studies, aiming to describe the $Al_xGa_{(1-x)}As$ complex

refractive index, $N(\omega) = n(\omega) - ik(\omega)$ (or the dielectric constant $\varepsilon = \varepsilon_1 - i\varepsilon_2$, where $\varepsilon_1 = n^2 - k^2$ and $\varepsilon_2 = 2nk$), as accurately as possible, can be found in the literature. Optical studies to determine the refractive index of liquid phase epitaxy (LPE) grown $Al_xGa_{(1-x)}As$ layers were first reported, covering the shorter wavelength range, between 1.2 eV and 1.8 eV[10] (690 nm–1030 nm) and from 1.5 eV to 6.0 eV[11] (205 nm–825 nm). van der Ziel and Gossard[12] reported transmission measurements extending the experimentally accessible range to 1.55 μm and above. However, most of their samples consisted of alternating GaAs/AlAs monolayers, and only one $Al_xGa_{(1-x)}As$ alloy was studied in detail ($x = 0.48$). Such alternating monolayers do not correspond to the alloys that have the same average Al content since they have an additional long-range periodic order in their growth direction, which is absent in the usual "random" alloys. This affects their bandgap and optical properties. Deri and Emanuel[13] developed a semi-empirical formula by combining a re-analysis of earlier $Al_xGa_{(1-x)}As$ index data with their own measurements of two samples, one in the direct bandgap region ($x = 0.203$) and one in the indirect bandgap region ($x = 0.5$), grown by metalorganic chemical vapor deposition (MOCVD).[13] Notably, by using a common equation to estimate Al content from PL data for all samples that were available in the literature at that time, and then fitting the data to a model by Adachi,[14] their work provided the first self-consistent tool for calculating the refractive index as a function of composition at technologically important telecom wavelengths of 1.3 μm and 1.55 μm. Meanwhile, Kaufman *et al.*[15] used a grating-coupling technique, to provide additional results in the short-wavelength range (0.76 μm–1.15 μm), on MBE-grown $Al_xGa_{(1-x)}As$ slab waveguides. Gehrsitz *et al.*[16] subsequently worked with $Al_xGa_{(1-x)}As$ alloys mainly grown by MOCVD and included in their study: one sample grown by MBE. They obtained extremely accurate ($\Delta n = 5 \times 10^{-4}$) experimental results from the modal propagation constants between 0.73 μm and 0.83 μm. Furthermore, they extended the wavelength range using transmission measurements of thin films after separating them from their substrates by selective etching. The precision of this technique strongly depends on the accuracy at which the film thickness and the interference order are known. The authors used the obtained 0.73 μm–0.83 μm refractive index dispersion to achieve that. In addition, they developed a modified Sellmeier[17] approximation by analyzing the refractive index of binary compounds (GaAs, GaP, and AlAs) and subsequently fitting their own experimental results of the $Al_xGa_{(1-x)}As$ ternaries to it. To find an analytic description as a function of chemical composition, wavelength, and temperature over the full composition range, they fitted polynomials to the compositional dependence of their fitting parameters to modify them appropriately. During this procedure, they observed a deviation in the bandgap region, resulting in a poor fit, only for the MBE-grown sample although the reason for that is not specified. Considerable theoretical research, mainly using semi-empirical models to calculate $Al_xGa_{(1-x)}As$ refractive indices as a function of x and λ, can be found in the literature.[18–22] The parameters of these models are simple functions of the composition, adapted to reproduce the available experimental data sets.

Two important review papers covering a wide range of III–V materials, including $Al_xGa_{(1-x)}As$, were released in 1985[23] and in 2001,[24] both of which stressed the need to keep revising the estimated values and to keep them up to date over the years. The latter goal has only been partly achieved as recent reports started providing revised refractive index values for some material systems, such as the $In_{1-x}Ga_xAs_yP_{1-y}$[25] and the $Al_xGa_{1-x}As_{0.5}Sb_{0.5}$ ($0.0 \le x \le 0.6$)[26] alloys that are lattice-matched to InP(100). However, a systematic study of the important MBE-grown $Al_xGa_{(1-x)}As$ layers has not been reported to date, despite $Al_xGa_{(1-x)}As$ being the most widely used alloy and MBE being one of the most prominent and widely used growth techniques at present, both in academia and industry. The only available MBE results[15] cover a very narrow spectral range, whereas the available results by other growth techniques (LPE or MOCVD) are also from 20 years ago or earlier and may not generally be applicable with the desired degree of accuracy.

This creates the necessity to obtain updated values since the increasing fabrication complexity of modern optoelectronic devices calls for an ever-increased modeling accuracy prior to the growth and fabrication runs. A very accurate III–V refractive index knowledge has been recently shown to be critical in device modeling for laser applications[27] and novel DFB designs,[28] especially in hybrid III–V laser structures on a Si substrate,[5,29,30] in which very small index inaccuracies may lead to erroneous results with respect to modal confinement factors and III–V to Si evanescent waveguide coupling. Such devices require a great deal of work to design, grow, and fabricate, and modeling errors are, thus, very costly. A large variety of other optoelectronic applications, such as detectors, modulators, and photovoltaic cells, also require this knowledge.

Modern MBE systems produce epitaxial layers of an extremely high quality and homogeneity as well as improved sharp interfaces between successive layers.[5] Our expectation, which further motivated the present work, is that these may lead to some differences in their refractive indices from samples grown many years ago by other growth techniques, especially for ternary and quaternary compounds. For example, inhomogeneities (Al concentration fluctuations within an AlGaAs sample) have been discussed as a source of potential systematic errors,[16] which are difficult to quantify. Further discrepancies from published data may be expected due to the superior current quality of the crystalline structure with a lower defect density and a better uniformity through thick layers. There are different conceivable ways in which such crystal (in)homogeneities could potentially influence the refractive index as well as the accuracy of its determination, the most important of which we will review in Sec. IV. In this respect, it is at present difficult to directly assess the exact structural details that may result from each different growth technique and their precise impact on n. It is, therefore, good practice to acquire reference results for each growth technique, over a wide spectral range, and to compare them. In addition, the better control that we now have over the exact thickness and composition in each epi-layer facilitates more accurate refractive index measurements by reducing the uncertainty of these parameters during the subsequent refractive index model fitting process. For example, in successive model fitting runs, some of the well-known parameters can be fixed, thereby reducing the free parameters of the model. We find that this procedure also provides a good way to control self-consistency in successive runs by fixing different parameters.

In this paper, we report our results on the growth and refractive index measurement of a series of MBE-grown $Al_xGa_{(1-x)}As$ ternary alloys, with a focus on the transparent wavelength region

(extinction coefficient $k \approx 0$) in which most optoelectronic devices operate. The refractive indices were measured using spectroscopic ellipsometry, and the data fitting parameters were analyzed by additional high-resolution x-ray diffraction (HRXRD) and photoluminescence (PL) measurements that we performed on the same samples. Ellipsometric measurements and data analysis were carried out independently with two different ellipsometry instruments in two international universities to ensure repeatability, resulting in a high degree of accuracy in our results. In Sec. IV of this paper, we provide a comprehensive comparison with previous results collected from the available literature sources. Our samples cover, fairly uniformly, the entire direct-bandgap composition region ($x < 0.4$) and slightly above.

II. SAMPLE PREPARATION AND MEASUREMENTS

The investigated samples were grown using a solid-source Veeco Gen-930 MBE system on p-doped ~7.5 h 10^{18} cm^{-3} (Zn) GaAs (100) substrates. A 200-nm thick, undoped GaAs buffer layer was grown on all GaAs substrates, except for one reference sample. As reference samples, we used two individual GaAs substrates, the first one without growing any buffer layer ("sample 1") and the second with a GaAs buffer layer grown on top of it by MBE ("sample 2"). Sample 2 served to check whether there are any observable differences between the MBE grown GaAs layer and that of the substrate wafer. $Al_xGa_{(1-x)}As$ layers were grown on five individual substrates, on top of the buffer layer, with the Al fraction increased from sample to sample (samples 3–7), as detailed in Table I. The AlGaAs layers were uncapped. All MBE-grown layers were nominally undoped. Some non-intentional doping (n.i.d) of the order of $5\,7 \times 10^{14}$ cm^{-3} is typically found in such AlGaAs alloys grown by MBE on GaAs substrates, but such low background doping is known to have a negligible influence on the optical properties of the samples,[25] and it is, therefore, not considered in the present work. The back side of all the samples was rough (not polished).

In order to obtain high-quality materials, we have grown the AlGaAs layers at high temperature with an enhanced chamber cleaning procedure, by cooling the MBE chamber for more than 1 week with liquid nitrogen (LN_2). Due to our previous experience in growing AlGaAs layers in multi-layer structures, we approximately knew the optimal growth conditions for our MBE to start with. Further optimization was performed by multiple growth runs and PL inspections of the samples until optimal PL characteristics (highest PL intensity and lowest FWHM) were achieved. We further confirmed, with low-temperature PL measurements, that there are no additional defect-related peaks.

The grown layers were initially characterized by HRXRD to determine their precise composition prior to ellipsometry measurements, as well as using PL to determine their effective bandgap. HRXRD data yield a precise compositional analysis over the complete composition range (in contrast to PL or optical absorption measurements) and can provide additional information on the strain of the layer.[31] Typical obtained HRXRD ω-2θ rocking curves are shown in Fig. 1, while Table I summarizes the measured compositions, the PL wavelength (energy), the thickness, and the lattice mismatch for all the studied $Al_xGa_{(1-x)}As$ samples. The narrow linewidths of the $Al_xGa_{(1-x)}As$ peaks in the diffraction data are a signature of the high quality of the ternary material. The peaks of the industrially made binary GaAs substrate have a slightly narrower linewidth, as expected. The thicknesses denoted for all samples are the ones obtained by our ellipsometry model best fit, in which initial estimated values were provided from the calibrated MBE growth rate. The thickness for sample 2 is the buffer layer thickness whereas for samples 3–7, it is the $Al_xGa_{(1-x)}As$ thickness only. All measurements were performed at room temperature (RT), $20 \pm 0.5\,^{\circ}C$.

Ellipsometry is a well-established, non-destructive optical technique that is widely used to measure the optical constants of thin films and bulk crystals, as is well-documented in the literature.[26,32–38] It has several advantages over conventional reflectivity techniques in terms of accuracy of the data. In summary, ellipsometry characterizes how the light polarization p- (electric field in the plane of incidence) and s- (normal to the plane of incidence) components change upon reflection (or transmission) in relation to each other. A known polarization is reflected off from the studied sample, and the output polarization is compared to the input. In general, reflection causes a change in the relative phases and amplitudes of the p and s waves that are characterized by the measured ellipsometric angles Δ and Ψ, respectively. The change in polarization in the ellipsometry measurement is commonly written in the form

$$\rho = \frac{r_p}{r_s} = \tan(\Psi)\exp(i\Delta) \tag{1}$$

TABLE I. Measured parameters of the studied $Al_xGa_{(1-x)}As$ ternary alloys.[a]

Sample #	Al fraction	PL wavelength	Thickness	Lattice constant (Å)	Lattice mismatch (%)
1	0	889 nm (1.395 eV)	Substrate	5.65338	...
2	0	890 nm (1.393 eV)	200 nm	5.65338	0.0000
3	0.097	819 nm (1.513 eV)	518 nm	5.65414	0.0135
4	0.219	729 nm (1.701 eV)	545 nm	5.65514	0.0311
5	0.342	669 nm (1.853 eV)	528 nm	5.65612	0.0484
6	0.411	640 nm (1.937 eV)	524 nm	5.65608	0.0478
7	0.452	624 nm (1.987 eV)	530 nm	5.65707	0.0652

[a]Al fraction as measured by HRXRD, PL peak wavelength (energy), $Al_xGa_{(1-x)}As$ layer thickness, lattice constant, and lattice mismatch with the substrate. The thickness for sample 2 is the GaAs buffer layer thickness whereas for samples 3–7, it is the $Al_xGa_{(1-x)}As$ thickness only (not the total AlGaAs + buffer thickness).

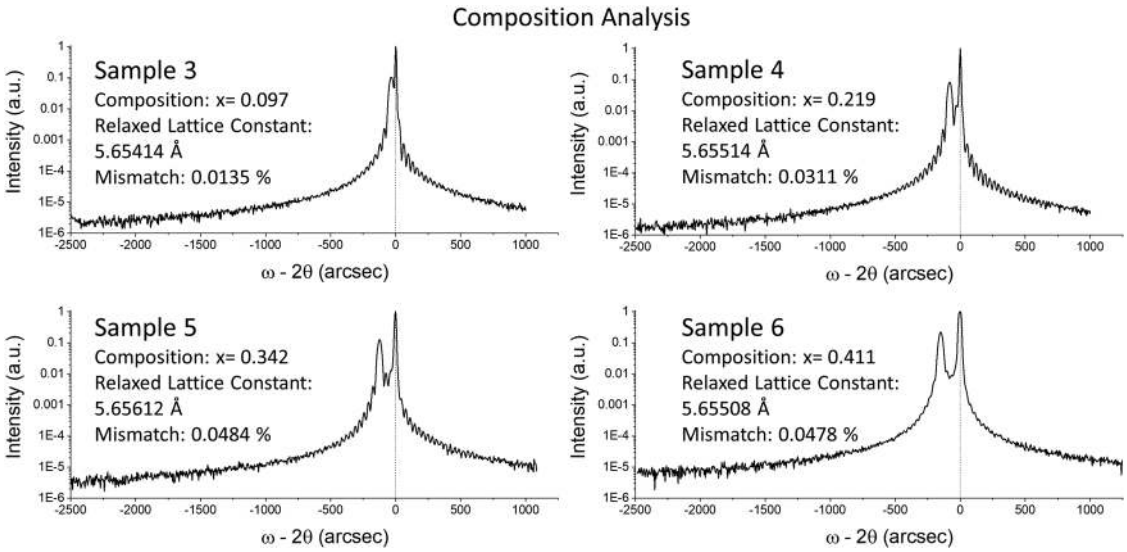

FIG. 1. Typical HRXRD ω-2θ scans obtained for the composition analysis of samples 3–6. Similar curves were obtained for all the samples, and the results are shown analytically in Table I.

where ρ is the complex reflection ratio between the Fresnel reflection coefficients of the p- (r_p) and s- (r_s) polarized waves at a given angle and energy.[39]

In the case of a bulk material having a perfect discontinuity with the ambient material (two-phase model), the dielectric function $\varepsilon(\omega)$ is directly related to the measured ratio, ρ, and may be obtained in a closed form.[39,41] This would also be the case in a multilayer structure if the layer thicknesses and optical properties are known for all layers except for one. Then, the real and imaginary parts of ε can be determined by direct numerical inversion at each wavelength independently.[40] However, such a solution assumes that there are "perfect" layers and interfaces and that there are no surface oxide layers of any type,[39,41] which is not a good model of semiconductor samples. Therefore, to analyze the ellipsometric data, a realistic layer structure model is necessary. In this case, results may be directly obtained for each composition at all probing wavelengths by an internally consistent measurement-fitting procedure. In our study, we used a wide range of probing wavelengths to ensure a high consistency of the models we used. We will describe the details of these models in Sec. III.

The ellipsometers were calibrated immediately before the measurements using a reference pure substrate sample. The fitting of the ellipsometry data was performed using the specialized software provided with these ellipsometers, and it was assisted by our precise knowledge of the materials' compositions and bandgaps, as obtained by HRXRD and PL.

Initial spectroscopic ellipsometry measurements on the MBE-grown $Al_xGa_{(1-x)}As$ ternary alloys were carried out on a Semilab SE-2000 variable angle spectroscopic ellipsometer at an angle of incidence of 75°, close to the Brewster angle of the substrate, at University College London (UCL), denoted hereafter as "Semilab" measurements. The ellipsometer uses a rotating compensator configuration, which consists of the following elements in consecutive order: a broadband white light source, polarizer, rotating compensator, microspot objective, analyzer, and detector. The focusing optics have a spot size of ~300 μm at 75° angle of incidence (AOI). To optimize the quality of ellipsometric data being collected, measurements were performed at a wide wavelength range of 250 nm–1650 nm and at various selected angles between 50° and 75°.[42] In the 245 nm–990 nm wavelength range, the Semilab ellipsometer employs a CCD spectrograph with an FWHM bandwidth less than 3 nm over the whole spectral range, whereas for the long-wavelength range (900 nm–1700 nm), a one-stage Peltier cooled InGaAs linear array detector with 256 pixels is used – the linear dispersion is of the order of 0.8 nm/pixel. Data analysis was performed using Semilab's "Spectroscopic Ellipsometry Analyzer (SEA)," software version 1.6.2.

The second series of measurements were performed using a Horiba Uvisel spectroscopic phase-modulated ellipsometer at the Polytechnic University of Valencia (UPV), denoted hereafter as "Horiba" measurements. Spectroscopic ellipsometry measurements in this case were performed in the 250 nm–2050 nm spectral range, at an incident angle of 70°. This ellipsometer incorporates photoelastic devices to modulate the polarization of the light emitted by a 75 W Xe short arc lamp. Calcite prisms are used to polarize the incident beam and to analyze the one reflected by the sample. Dedicated DeltaPlus2 software was used for data acquisition, modeling, and reporting. Measurements were performed at 5 distinct positions on each sample.

To define a proper basis for building the ellipsometric models, the uncoated reference substrates were first measured. This enabled the accurate collection of n, k data for the substrate and calibration of a thin native oxide layer that develops on GaAs surfaces when they are exposed to the atmosphere, using a simple ellipsometry fitting model. To do so, we measured a substrate before and after cleaning the surface with HCl, a process known to fully remove the

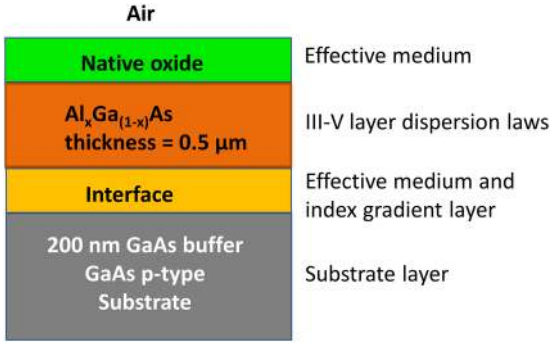

FIG. 2. Schematic cross-sectional view of the layer model used for fitting the ellipsometric data. The substrate and buffer layers were first calibrated using our reference samples 1 and 2, and the obtained *n*, *k* data were used as input in our fitting models for the $Al_xGa_{(1-x)}As$ layers.

native oxide from a GaAs surface. For cleaning, the entire sample was immersed into 37% HCl for 1 min, subsequently rinsed with deionized water, and dried with nitrogen flow. When the measurement is performed immediately (within ~1 min) after HCl cleaning, it can be assumed that virtually no oxide is present on the surface.[5] Subsequently, the $Al_xGa_{(1-x)}As$ samples were measured. For $Al_xGa_{(1-x)}As$ layers, this surface treatment would not guarantee a completely oxide-clean surface; therefore, a surface oxide layer was employed in our respective models (Fig. 2), as will be detailed in Sec. III. If the surface oxide layers are not rigorously taken into account in the ellipsometry models, it leads to inaccuracies in the extracted optical constants, as also emphasized in other recent research.[39]

III. STRUCTURAL LAYER MODELS

The measured Ψ and Δ values were analyzed with a fitting procedure that enables an analytical description of the data with a high accuracy, using an appropriate layer structure model to describe each sample. The model is used to calculate the predicted response from Fresnel's equations, which describe reflection and transmission of *p*- and *s*-polarized light from each layer, given its thickness and optical constants. Thus, it calculates the Ψ_{mod} and Δ_{mod} values, given the light wavelength, λ, and the angle of incidence, Φ. If the values for a layer are not known, an estimate is given for the purpose of a preliminary calculation, and the calculated values are compared to the experimental data. The unknown material properties can then be varied to improve the match between Ψ, Δ and Ψ_{mod}, Δ_{mod}. The results of these theoretical calculations can be corrected by using different model options (such as incident angle shift, micro-spot correction, backside reflection, anisotropy, and depolarization) for a better description of the measurement. Finding the best match between the model and the experiment is achieved through regression, for which the specialized ellipsometer software was used. A fitting procedure to the experimental data is a multi-variable and highly nonlinear problem. The built-in regression algorithms (global and local optimizers) minimize a well-defined figure of merit (FOM) function, to determine the fitted parameters (structure and optical constants), their associated errors, covariance matrix, and quantitative characteristics for the goodness of fit (coefficients of determination and standard deviation). In our study, the differences between the measured (Ψ and Δ) and modeled (Ψ_{mod} and Δ_{mod}) spectra were quantified using the root mean square error (RMSE) value and the coefficient of determination, R^2.[43] To refine the calculated (modeled) results, we performed an interactive non-linear regression analysis to obtain fitting values that represent the best fit of the model to the measured data. Since ellipsometry is an indirect technique to measure the indices, when fitting many samples at a variety of wavelengths, consistency of the fitting parameters is a key feature besides fitting quality. In the present work, we have taken multiple additional measures to ensure consistency, as detailed below. Thus, the RMSE and R^2 parameters, as calculated by the ellipsometer fitting software (SEA) in each fitting session, are reliable measures of the fitting accuracies. For all the measurements that we present here, we obtained an R^2 higher than 0.98 and an RMSE lower than 1.

A simple schematic representing our model is shown in Fig. 2. As evidenced from the discussion above, an appropriate description of each layer is important such that parameterization of the optical constants and other variables can be carried out effectively in a physical and consistent way. The "*n*, *k* files" that were obtained from the reference "sample 2" were used as the model substrate for all samples. As shown in Fig. 2, an interface/diffusion layer was inserted in-between the substrate/buffer layer and the grown layers, to account for any material intermixing[27] that takes place within the first few to several AlGaAs monolayers during their epitaxial growth on GaAs. Therefore, the interface layer served as an index gradient layer between the GaAs/$Al_xGa_{(1-x)}As$ layers. In this structural layer model, the interface is to be regarded as a layer rather than a surface, with a thickness of a few to several monolayers (up to 4 nm).

Moreover, as discussed in Sec. II and shown in Fig. 2, we chose not to grow a GaAs cap layer on top of the structure. The reason was to avoid adding an additional interface and layer. Multiple interfaces are "harmful" to the ellipsometry analysis because it is difficult to measure the precise thickness of the intermixed region and potential inhomogeneities therein. We found that when dealing with "similar" material, say GaAs and $Al_{0.1}Ga_{0.9}As$, intermixing affects the ellipsometric data quality considerably, even for thick layers, and must be treated carefully in the fitting models. Even though an intermixed interface can indeed be treated fairly well with an appropriate model, multiple imperfect interfaces severely increase the number of fitting parameters, which makes the fitting much more complicated and thus introduces additional errors. The downside of not including the cap layer is the native oxide that is known to grow at the surface of semiconductors through contact with the atmosphere.[45] To account for it, a native oxide layer was included on the top surface for each sample in our models.[44] To appropriately deal with the oxide, the measurements were performed very shortly after the samples were removed from the MBE vacuum chamber, which ensures that the oxide is thin (especially since we are only using samples with $x < 0.45$), which makes the analysis easier. For the second series of measurements, the samples were transported in a vacuum container. Then, we achieved a first estimate of the oxide thickness, as well as reasonable ranges, using the literature, the Al content, and the time that it was exposed to the atmosphere until the measurement. Given the short time that $Al_xGa_{(1-x)}As$ was exposed, it was expected to have a thickness of a few to several nm and a refractive index of ~1.5

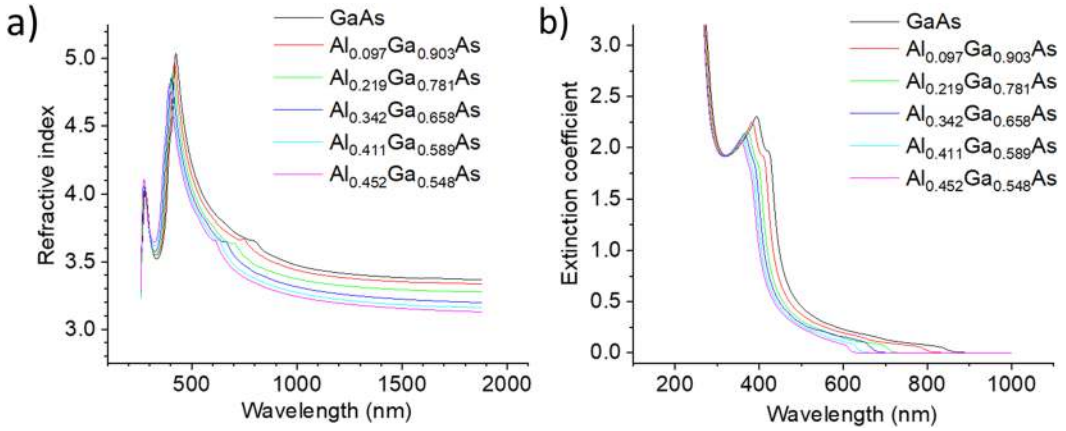

FIG. 3. (a) Refractive index dispersion as deduced with the Horiba ellipsometer in a wavelength range from 250 nm to 1900 nm. (b) The extinction coefficient as obtained in the same measurement.

for the samples with low Al-content.[44] For the higher Al-content ($x > 0.3$) samples, a mixture of three oxides, Al_2O_3, As_2O_3, and Ga_2O_3, with a higher thickness is generally present[46] and was included in the model for samples 5–7. This layer was simulated using the "effective medium" method.[47,48] This model also encompasses the presence of roughness, which drastically improved the goodness-of-fit (RMSE and R^2) parameters.

The main part of the calculation concerns the $Al_xGa_{(1-x)}As$ layer "dispersion laws" for n and k, for which we have investigated several dispersion models, embedded in the employed software. "Dispersion laws" are mathematical formulae developed to model the optical properties of materials. Using appropriate dispersion models is important. The model should ideally use a small number of fitting parameters, most of which would have a physical significance, for example, by corresponding to critical points in the band structure. The success of the parameterization strongly depends on the choice of the most suitable method with the least possible parameters. A proper approach is to start with the most robust models that use a small number of fit parameters and to refine them with more sophisticated approaches using the previously determined parameters as starting parameters, or as a guide to define reasonable ranges for the parameter search.[56] If the parameters have a physical significance, the fitting is more likely to follow a correct path as the corresponding parameters may be fixed at values obtained using supplementary measurements in the first steps of this iterative process, as we have performed in this work.

We evaluated these models' compatibility to our material system based on the fitting quality and self-consistency of the results as provided by each model. The models that provided the most accurate outcome are those of Forouhi and Bloomer[49,50] (FB) and the model of Tanguy.[51,52] Even though, for application-related purposes, our main focus has been on the transparent region, we, in fact, found these two models very useful for the whole range. We note that as long as the energy (wavelength) range of interest to determine n starts sufficiently lower than the bandgap, E_g, the modified Sellmeier approach[16] also worked particularly well for our measurements, but if the whole range is included, the fitting slightly deteriorates, and for wavelengths very close to the bandgap, the Sellmeier dispersion model becomes inaccurate. The models generate refractive index results that are virtually identical below the bandgap to within the experimental error of our extraction method; hence, in Figs. 3–6, we show the fitting obtained from the FB model that gave the best RMSE. Details of these models may be found in the cited literature. Here, we present a brief summary, highlighting their main concepts that are important for our analysis.

Forouhi and Bloomer performed a quantum mechanical treatment based on a one-electron model with a finite lifetime for the electron excited state. Their model derives an expression for the

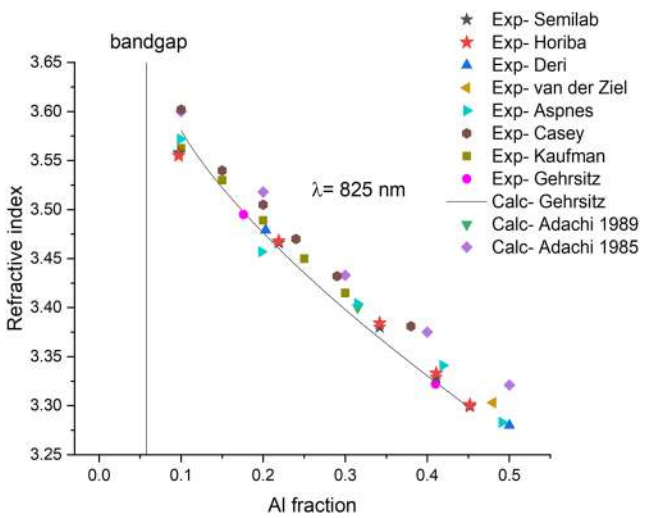

FIG. 4. Summary of our refractive index results at 825 nm and comparison with the available literature (Deri and Emanuel,[13] van der Ziel and Gossard,[12] Aspnes *et al.*,[11] Casey *et al.*,[10] Kaufman *et al.*,[15] Gehrsitz *et al.*,[16] and Adachi *et al.*[21,23]). The red and black star symbols represent our experimental results. *We calculated the results shown for Gehrsitz *et al.*,[16] using their analytic description, which they obtained by fitting their experimental results.

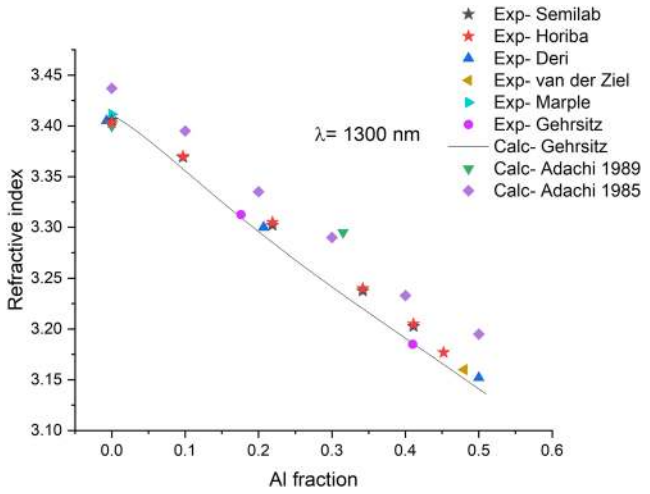

FIG. 5. Summary of our refractive index results at 1300 nm and comparison with the available literature (Deri and Emanuel,[13] van der Ziel and Gossard,[12] Marple,[55] Gehrsitz *et al.*,[16] and Adachi *et al.*[21,23]). The red and black star symbols represent our experimental results. *For the calculated results shown for Gehrsitz *et al.*,[16] the same method as in Fig. 4 is used.

quantum states that are responsible for the absorption peaks and edges in the $k(E)$ spectrum and their respective amplitudes. Using a semi-empirical method for fitting their coefficients to measured data, and subsequently using the Kramers–Kronig relations, the real part $n(E)$ is obtained as the Hilbert transform of $k(E)$. Their method was previously tested in binary materials and showed an excellent accuracy in a variety of both amorphous[50] (single k-peak) and crystalline[49] materials [multiple peaks in the $k(E)$ spectrum].

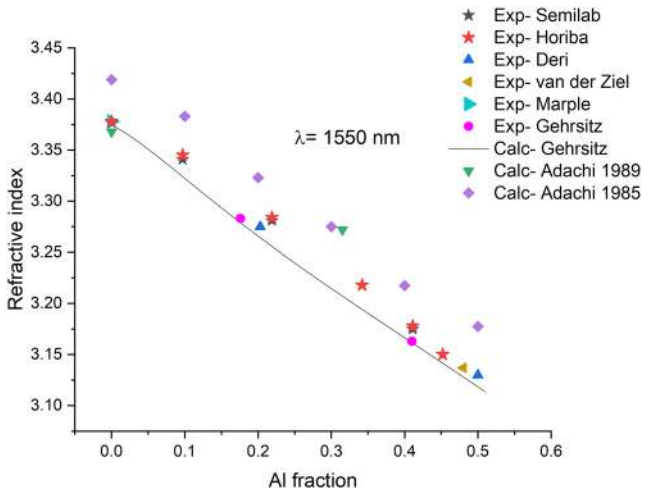

FIG. 6. Summary of our refractive index results at 1550 nm and comparison with the available literature (Deri and Emanuel,[13] van der Ziel and Gossard,[12] Marple,[55] Gehrsitz *et al.*,[16] and Adachi *et al.*[21,23]). The red and black star symbols represent our experimental results. *For the calculated results shown for Gehrsitz *et al.*,[16] the same method as in Fig. 4 is used.

Tanguy's model focuses on including the influence of excitonic effects[52,53] in the calculation of the real part of the dielectric constant, thus improving on earlier models. The main advantages of this semi-empirical analytical model lie in its accuracy near E_g as well as in the transparency region and in the relatively small number of physical parameters involved, most of them being accessible from measurements in the transparency region, where the error in n can be very small.[51] A major advantage of both dispersion models is that they are consistent with the Kramers–Kronig (KK) relations, which means that theoretically, when k as a function of E is known (at all energies), n can be fully determined. This has not been the case with most previous formulations of $N(E)$, which did not capture its k-dependence, and for this reason, their formulations for optical dispersion relations of crystalline semiconductors and dielectrics appear more complicated.[49] The KK relations, also known as dispersion relations, are very important because they stem directly from the principle of causality (no signals can be transmitted through a medium at a speed greater than that of light in vacuum). This leads to the $N(E) = n(E) - ik(E)$ analytic behavior and, thus, to a fundamental relation between its real, $n(E)$, and imaginary, $k(E)$, parts.[54] The dispersion relations as developed in the above-mentioned papers not only describe optical constants of crystalline semiconductors but may also guide their accurate experimental determination.

To correctly account for absorption resonances that lie outside the measured spectral range when applying the KK relations, it is important to include an additional constant term to the formulae of the dispersion models.[50] In our approach, this term is treated as an additional free fitting parameter. It aims to collectively represent the contributions of such resonances in the ultraviolet or far-infrared regions to the dispersion. The effect of absorption out of the investigated photon energy range could alternatively be considered by adding Sellmeier oscillators placed at the appropriate IR and UV regions of the spectrum.

IV. RESULTS AND DISCUSSION

The refractive index, n, wavelength dependent in the wavelength range from 250 nm to 1900 nm as obtained with the Horiba ellipsometer for all samples, is shown schematically in Fig. 3(a). Figure 3(b) shows the extinction coefficient, k, which was obtained in the same spectral range. The region 1000 nm–1900 nm is not shown in Fig. 3(b) as $k \approx 0$ for all samples. The most important results are summarized in Table II, which reports our measured refractive indices at three technologically important wavelengths (825 nm, 1300 nm, and 1550 nm). In addition, it is worth noting that using the semi-empirical formula proposed by Gehrsitz *et al.*,[16] we calculated that the refractive index varies by approximately 0.6% ($\Delta n \sim 0.02$) for a temperature change of 100 K. Figure 4 shows our results for the refractive index as a function of the Al content at $\lambda = 825$ nm, and in the same plot, we show previously reported values for comparison, whereas Fig. 5 summarizes the results at $\lambda = 1300$ nm and Fig. 6 at $\lambda = 1550$ nm. In Figs. 4–6, our own results are shown using the red (Horiba) and black (Semilab) star symbols, whereas the other used symbols represent results from the literature.

It is worth noting that much more data are available in the literature in the shorter wavelength range around $\lambda = 825$ nm, despite the fact that a great deal of potential applications is now arising at

TABLE II. Refractive index values of our samples at 825 nm, 1300 nm, and 1550 nm.[a]

	Ref index at 825 nm		Ref index at 1.3 μm		Ref index at 1.55 μm	
Material	Semilab	Horiba	Semilab	Horiba	Semilab	Horiba
GaAs	3.610	3.606	3.406	3.403	3.377	3.378
$Al_{0.097}Ga_{0.903}As$	3.558	3.555	3.369	3.370	3.341	3.345
$Al_{0.219}Ga_{0.781}As$	3.466	3.468	3.302	3.305	3.281	3.284
$Al_{0.342}Ga_{0.658}As$	3.380	3.384	3.238	3.240	3.218	3.218
$Al_{0.411}Ga_{0.589}As$	3.329	3.333	3.203	3.205	3.175	3.178
$Al_{0.452}Ga_{0.548}As$	3.299	3.301	3.177	3.177	3.150	3.150

[a]As measured independently using Semilab and Horiba ellipsometers.

λ = 1300 nm and at λ = 1550 nm, especially in the field of hybrid lasers for optical interconnects. At λ = 825 nm, we also find the closest agreement between our results and some of those provided by earlier reports. At this wavelength, we see very good agreement with the results of Gehrsitz *et al.*[16] for all compositions except for $x = 0.097$ (sample 3) that lies very close to the bandgap. The regions near and above the bandgap are harder to assess, but we consider our results to be accurate for the reasons discussed above. Moreover, our 825 nm results agree well with those of Kaufman *et al.*,[15] which is the only systematic work on MBE-grown alloys that we are aware of, but their results are limited to short wavelengths; hence, we are unable to extend this comparison to 1.3 μm and 1.55 μm. Across the whole wavelength range, our results are systematically lower than those of the models by Adachi *et al.*,[21,23] which we think tend to overestimate the refractive index by about 2%. At the telecom wavelengths, our results exhibit a similar trend to previous theoretical models by Gehrsitz *et al.*[16] and Adachi *et al.*,[21,23] but we observe mild but clear differences with both, albeit smaller with the former, in the moderate Al fraction region. As it may be seen from Figs. 5 and 6, very few previous experimental results are available in this range. Comparing with these, we can see that our results are in fairly good agreement with the single experimental points of Deri and Emanuel[13] and van der Ziel and Gossard.[12] Our results are the first systematic experimental work for MBE $Al_xGa_{(1-x)}As$ alloys at these wavelengths, and they fill-in the missing gaps to uniformly cover the whole technologically relevant composition range ($x < 0.45$) and may thus serve as a reference study for this material system. This has been lacking, and there was, prior to this work, some uncertainty as to how accurately the material libraries – made out mainly from theoretical models and some previously studied alloys that were grown by other techniques – could serve for that purpose. Our main conclusion is that the previous studies using alloys grown by LPE and MOCVD do indeed agree fairly well with our obtained results at the shorter wavelengths, especially in the low Al-concentration region. Near the telecom wavelengths, at the moderate-Al fraction region, we find some differences of the order of 1% with some of the previous experiments and models that are widely-used as references. Such differences are important for certain applications, such as hybrid III–V lasers on silicon in which an accuracy of the order of 0.1% is desired. For most applications, it is in general highly beneficial to have a knowledge as accurate as possible. We believe that our results provide the most accurate reference for the MBE-grown $Al_xGa_{(1-x)}As$ samples as we have performed dedicated measurements and fitting exactly at the suitable wavelengths for the aforementioned applications, rather than extrapolating data obtained in different wavelength regions.

As also seen in Figs. 5 and 6, the scatter amongst the previously reported data from different sources is sometimes significant, and it often exceeds the uncertainty for their own measurements when it is defined. This issue has already been discussed in the literature.[13,15,16] It is difficult to exactly determine the precise reasons for the differences in refractive index determination in different literature sources, especially since a variety of growth and measurement techniques have been used. We will, however, attempt to pinpoint some of the important sources that might be in play. The primary one is the insufficiently accurate composition determination of some sources, when that was obtained by optical techniques, as also explained previously.[13,15,16] We believe that, in addition, there might be issues regarding the composition homogeneity, arising from the different growth techniques that have been used to prepare the $Al_xGa_{(1-x)}As$ layers. One mechanism for inhomogeneous composition is short range clustering. There is substantial literature on short range clustering in AlGaAs with low temperature vapor phase growth, but there are no reports on MBE growth on (100) surfaces.[15,56] Such inhomogeneities may affect the refractive index determination accuracy in several ways. For example, some vertical inhomogeneity would create wavelength-dependent measurement artifacts in ellipsometry because the penetration depth of the illuminating light is different for each of the constituent wavelengths and the sample optical properties are integrated over different depths.[57]

Our obtained refractive index values between the Semilab and Horiba measurements are very similar ($\Delta n < 5 \times 10^{-3}$ in the transparent region), which is of the order of the experimental uncertainty, and they were reproducible for measurements taken at different spots in each sample. Therefore, we propose that the average value of these results for the refractive index of MBE-grown $Al_xGa_{(1-x)}As$ may be used with a high degree of confidence in the future work. These are summarized in Table III. Our interactive non-linear regression method that we used allowed us to fix or vary different model parameters in successive fitting runs, which allowed us to control the consistency of a model. This method becomes particularly useful when some of the parameters can also be reliably obtained using other independent techniques, for example, the composition of our films as estimated from spectroscopic ellipsometry

TABLE III. Summary of the MBE-grown $Al_xGa_{(1-x)}As$ refractive index values at 825 nm, 1300 nm, and 1550 nm as extracted from the current study.[a]

Material	Ref index at 825 nm	Ref index at 1.3 μm	Ref index at 1.55 μm
GaAs	3.608	3.405	3.378
$Al_{0.097}Ga_{0.903}As$	3.557	3.370	3.343
$Al_{0.219}Ga_{0.781}As$	3.467	3.304	3.283
$Al_{0.342}Ga_{0.658}As$	3.382	3.239	3.218
$Al_{0.411}Ga_{0.589}As$	3.331	3.204	3.177
$Al_{0.452}Ga_{0.548}As$	3.300	3.177	3.150

[a]Our final proposed values are the average of those obtained using Semilab and Horiba ellipsometers that are presented in Table II.

fitting when allowed to vary in some given runs was very close to that determined by HRXRD. A second control parameter of the self-consistency of our method was provided by the PL measurements. In this regard, it should be noted that as was explicitly shown in a careful study combining absorption measurements with PL on $Al_xGa_{(1-x)}As$ alloys, the PL peaks underestimate the optical bandgap (threshold for photons to be absorbed) in $Al_xGa_{(1-x)}As$ by up to 30 meV for undoped samples,[58] corresponding to $\Delta x \sim 0.02$. Thus, following the study by Moemar *et al.*,[58] during our consistency evaluation, the PL wavelength was corrected upward by 20 meV–30 meV, the exact value depending on the composition and temperature, in order to compare it to the fitted fundamental bandgap, E_g values in the dispersion models, and the corresponding Al-content of the alloy.[13,58] Given this correction, our results, for p-doped GaAs and undoped $Al_xGa_{(1-x)}As$, are in very good agreement with the composition dependence of the direct bandgap as extracted by Bosio *et al.*[59] and Miller *et al.*[60]

V. CONCLUSIONS

In conclusion, we provide refractive index values over a wide spectral range below the bandgap for $Al_xGa_{(1-x)}As$ ternary alloys, grown using MBE and measured using spectroscopic ellipsometry. We find slightly different values in our MBE grown alloys compared to those grown by LPE or MOVCD previously reported in the literature, as well as to semi-empirical models aiming to calculate the refractive index as a function of the Al content. Such differences, of the order of 1%, can be important for a number of applications, especially those dealing with III–V to Si evanescent waveguide coupling in hybrid optoelectronic devices where small index changes strongly affect the mode profiles. The accuracy of our measurements has been improved using the following methodology: (a) by using state-of-the-art growth and measurement equipment, (b) by cross-checking our ellipsometric model parameters (alloy composition and bandgap) using HRXRD and PL measurements that were fed back into our models, and (c) repeating the measurements independently at two international universities using different pieces of equipment and model fitting software to ensure a high level of consistency. Our results will, thus, be useful in future heterostructure designs employing such alloys.

ACKNOWLEDGMENTS

This work was supported by EU H2020 L3MATRIX. The L3MATRIX project is co-funded by the Horizon 2020 Framework Program of the European Union, with Grant Agreement No. 688544. The L3MATRIX project is an initiative of the Photonics21 Public Private Partnership.

DATA AVAILABILITY

The data that support the findings of this study are available from the corresponding author upon request.

REFERENCES

[1]P. C. H. Poon, L. G. Commander, D. R. Selviah, and M. G. Robinson, "Extension of the useful focal length range of microlenses by oil immersion," J. Opt. A **1**(2), 133 (1999).
[2]L. G. Commander, S. E. Day, and D. R. Selviah, "Variable focal length microlenses," Opt. Commun. **177**(1-6), 157–170 (2000).
[3]R. Mussina, D. R. Selviah, F. A. Fernandez, A. G. Tijhuis, and B. P. de Hon, "A rapid accurate technique to calculate the group delay, dispersion and dispersion slope of arbitrary radial refractive index profile weakly-guiding optical fibers," Prog. Electromagn. Res. **145**, 93–113 (2014).
[4]H. Baghsiahi, K. Wang, W. Kandulski, R. C. A. Pitwon, and D. R. Selviah, "Optical waveguide end facet roughness and optical coupling loss," J. Lightwave Technol. **31**(16), 2959–2968 (2013).
[5]S. Chen, W. Li, J. Wu, Q. Jiang, M. Tang, S. Shutts, S. N. Elliott, A. Sobiesierski, A. J. Seeds, I. Ross, P. M. Smowton, and H. Liu, "Electrically pumped continuous-wave III–V quantum dot lasers on silicon," Nat. Photonics **10**, 307–311 (2016).
[6]J. L. Jewell, J. P. Harbison, A. Scherer, Y. H. Lee, and L. T. Florez, "Vertical-cavity surface-emitting lasers: Design, growth, fabrication, characterization," J. Quantum Electron. **27**, 1332 (1991).
[7]L. Sapienza, M. Davanco, A. Badolato, and K. Srinivasan, "Nanoscale optical positioning of single quantum dots for bright and pure single-photon emission," Nat. Commun. **6**, 7833 (2015).
[8]H. Sakata and S. Takeuchi, "Grating-assisted directional coupler filters using AlGaAs/GaAs MQW waveguides," IEEE Photonics Technol. Lett. **3**, 899 (1991).
[9]N. Vandamme, H.-L. Chen, A. Gaucher, B. Behaghel, A. Lemaître, A. Cattoni, C. Dupuis, N. Bardou, J.-F. Guillemoles, and S. Collin, "Ultrathin GaAs solar cells with a silver back mirror," IEEE J. Photovoltaics **5**(2), 565–570 (2015).
[10]H. C. Casey, D. D. Sell, and M. B. Panish, "Refractive index of $Al_xGa_{1-x}As$ between 1.2 and 1.8 eV," Appl. Phys. Lett. **24**, 63 (1974).
[11]D. E. Aspnes, S. M. Kelso, R. A. Logan, and R. Bhat, "Optical properties of Al_xGa_1 −x As," J. Appl. Phys. **60**, 754 (1986).
[12]J. P. van der Ziel and A. C. Gossard, "Absorption, refractive index, and birefringence of AlAs–GaAs monolayers," J. Appl. Phys. **48**, 3018 (1977).
[13]R. J. Deri and M. A. Emanuel, "Consistent formula for the refractive index of $Al_xGa_{1-x}As$ below the band edge," J. Appl. Phys. **77**, 4667 (1995).
[14]S. Adachi, "Optical properties of $Al_xGa_{1-x}As$ alloys," Phys. Rev. B **38**, 12345 (1988).
[15]R. G. Kaufman, G. R. Hulse, D. J. Vezzetti, A. L. Moretti, K. A. Stair, G. P. Devane, and T. E. Bird, "Measurement of the refractive index of $Al_xGa_{1-x}As$ and the mode indices of guided modes by a grating coupling technique," J. Appl. Phys. **75**, 8053 (1994).
[16]S. Gehrsitz, F. K. Reinhart, C. Gourgon, N. Herres, A. Vonlanthen, and H. Sigg, "The refractive index of $Al_xGa_{1-x}As$ below the band gap: Accurate determination and empirical modeling," J. Appl. Phys. **87**, 7825 (2000).
[17]H. Fujiwara, *Spectroscopic Ellipsometry: Priciples and Applications* (John Wiley & Sons, Ltd., 2007).
[18]J. Zheng, C.-H. Lin, and C. H. Kuo, J. Appl. Phys. **82**, 792 (1997).
[19]Y. Kokubo and I. Ohta, "Refractive index as a function of photon energy for AlGaAs between 1.2 and 1.8 eV," J. Appl. Phys. **81**, 2042 (1997).
[20]D. W. Jenkins, "Optical constants of $Al_xGa_{1-x}As$," J. Appl. Phys. **68**, 1848 (1990).

[21] S. Adachi, "Optical dispersion relations for GaP, GaAs, GaSb, InP, InAs, InSb, $Al_xGa_{1-x}As$, and $In_{1-x}GaxAsyP_{1-y}$," J. Appl. Phys. **66**, 6030–6040 (1989).
[22] U. Das and P. K. Bhattacharya, J. Appl. Phys. **58**, 341 (1985).
[23] S. Adachi, "GaAs, AlAs, and $Al_xGa_{1-x}As$: Material parameters for use in research and device applications," J. Appl. Phys. **58**, R1 (1985).
[24] I. Vurgaftman, J. R. Meyer, and L. R. Ram-Mohan, "Band parameters for III-V compound semiconductors and their alloys," J. Appl. Phys. **89**, 5815–5875 (2001).
[25] S. Seifert and P. Runge, "Revised refractive index and absorption of $In_{1-x}Ga_xAs_yP_{1-y}$ lattice-matched to InP in transparent and absorption IR-region," Opt. Mater. Express **6**(2), 251691 (2016).
[26] S. G. Choi, G. C. Hillier, and J. G. J. Adams, "Ellipsometric studies of $Al_xGa_{1-x}As_{0.5}Sb_{0.5}$ ($0.0 \le x \le 0.6$) alloys lattice-matched to InP(100)," J. Appl. Phys. **115**, 023510 (2014).
[27] K. Papatryfonos, G. Rodary, C. David, F. Lelarge, A. Ramdane, and J.-C. Girard, "One-dimensional nature of InAs/InP quantum dashes revealed by scanning tunneling spectroscopy," Nano Lett. **15**(7), 4488–4497 (2015).
[28] K. Papatryfonos, D. Saladukha, K. Merghem, S. Joshi, F. Lelarge, S. Bouchoule, D. Kazazis, S. Guilet, L. Le Gratiet, T. J. Ochalski, G. Huyet, A. Martinez, and A. Ramdane, "Laterally coupled distributed feedback lasers emitting at 2 μm with quantum dash active region and high-duty-cycle etched semiconductor gratings," J. Appl. Phys. **121**, 053101–053108 (2017).
[29] Y. Hu, D. Liang, K. Mukherjee, Y. Li, C. Zhang, G. Kurczveil, X. Huang, and R. G. Beausoleil, "III/V-on-Si MQW lasers by using a novel photonic integration method of regrowth on a bonding template," Light Sci. Appl. **8**, 93 (2019).
[30] J. Wang, Y. Bai, H. Liu, Z. Cheng, M. Tang, S. Chen, J. Wu, K. Papatryfonos, Z. Liu, Y. Huang, and X. Ren, "Optimization of 1.3 μm InAs/GaAs quantum dot lasers epitaxially grown on silicon: Taking the optical loss of metamorphic epilayers into account," Laser Phys. **28**(12), 126206 (2018).
[31] S. Gehrsitz, H. Sigg, N. Herres, K. Bachem, K. Köhler, and F. K. Reinhart, "The refractive index of $Al_xGa_{1-x}As$ below the band gap: Accurate determination and empirical modeling," Phys. Rev. B **60**, 11601 (1999).
[32] D. den Engelsen, "Ellipsometry of anisotropic films," J. Opt. Soc. Am. **61**, 1460 (1971).
[33] J. J. Yoon, T. H. Ghong, J. S. Byun, Y. D. Kim, D. E. Aspnes, H. J. Kim, Y. C. Chang, and J. D. Song, "Optical properties of $In_xAl_{1-x}As$ alloy films," Appl. Phys. Lett. **92**, 151907 (2008).
[34] J. J. Yoon, T. J. Kim, Y. W. Jung, D. E. Aspnes, Y. D. Kim, H. J. Kim, Y. C. Chang, S. H. Shin, and J. D. Song, "Dielectric functions and interband transitions of $In_{1-x}Al_xSb$ alloys," Appl. Phys. Lett. **97**, 111902 (2010).
[35] D. Serries, M. Peter, N. Herres, K. Winkler, and J. Wagner, "Raman and dielectric function spectra of strained $GaAs_{1-x}Sb_x$ layers on InP," J. Appl. Phys. **87**, 8522 (2000).
[36] T. J. Kim, J. J. Yoon, S. Y. Hwang, D. E. Aspnes, Y. D. Kim, H. J. Kim, Y. C. Chang, and J. D. Song, "Interband transitions of $InAs_xSb_{1-x}$ alloy films," Appl. Phys. Lett. **95**, 111902 (2009).
[37] J. Y. Kim, J. J. Yoon, T. J. Kim, Y. D. Kim, E. H. Lee, M. H. Bae, J. D. Song, W. J. Choi, C.-T. Liang, and Y.-C. Chang, "Optical properties of $AlAs_xSb_{1-x}$ alloys determined by in situ ellipsometry," Appl. Phys. Lett. **103**, 011901 (2013).
[38] S. G. Choi, C. J. Palmstrøm, Y. D. Kim, S. L. Cooper, and D. E. Aspnes, "Dielectric functions of $AlxGa_{1-x}Sb$ ($0.00 \leqslant x \leqslant 0.39$) alloys from 1.5 to 6.0 eV," J. Appl. Phys. **98**, 104108 (2005).
[39] A. Singh, Y. Li, B. Fodor, L. Makai, J. Zhou, H. Xu, A. Akey, J. Li, and R. Jaramillo, "Near-infrared optical properties and proposed phase-change usefulness of transition metal disulfides," Appl. Phys. Lett. **115**, 161902 (2019).
[40] *Handbook of Ellipsometry*, edited by H. G. Tompkins and E. A. Irene (William Andrew Publishing, Norwich, NY, 2005).
[41] S. Logothetidis, M. Cardona, and M. Garriga, "Temperature dependence of the dielectric function and the interband critical-point parameters of $Al_xGa_{1-x}As$," Phys. Rev. B **43**, 11950 (1991).
[42] J. A. Woollam, B. D. Johs, C. M. Herzinger, J. N. Hilfiker, R. A. Synowicki, and C. L. Bungay, "Overview of variable angle spectroscopic ellipsometry (VASE), Part I: Basic theory and typical applications," Proc. SPIE **10294**, 1029402 (1999).
[43] National Institute of Standard and Technology (NIST), Gaithersburg, MD 20899- 1070, USA: NIST/ SEMATECH e-Handbook of Statistical Methods, 2007, http://www.itl.nist.gov/div898/handbook/.
[44] H. G. Bukkems, Y. S. Oei, U. Richter, and B. Gruska, "Analysis of III-V layer stacks on INP substrates using spectroscopic ellipsometry in NIR spectral range," Thin Solid Films **364**(1-2), 165–170 (2000).
[45] S. Zollner, "Model dielectric function for native oxides on compound semiconductors," Appl. Phys. Lett. **63**(18), 2523–2524 (1993).
[46] M. V. Sukhorukova, I. A. Skorokhodova, and V. P. Khvostikov, "Ellipsometric study of ultrathin $Al_xGa_{1-x}As$ layers," Semiconductors **34**, 56 (2000).
[47] D. E. Aspnes, "Optical properties of thin films," Thin Solid Films **89**, 249 (1982).
[48] G. E. Jellison, Jr., L. A. Boatner, D. H. Lowndes, R. A. McKee, and M. Godbole, "Optical functions of transparent thin films of $SrTiO_3$, $BaTiO_3$, and SiO_x determined by spectroscopic ellipsometry," Appl. Opt. **33**, 6053 (1994).
[49] A. R. Forouhi and I. Bloomer, "Optical properties of crystalline semiconductors and dielectrics," Phys. Rev. B **38**(3), 1865 (1988).
[50] A. R. Forouhi and I. Bloomer, "Optical dispersion relations for amorphous semiconductors and amorphous dielectrics," Phys. Rev. **34**, 7018 (1986).
[51] C. Tanguy, "Refractive index of direct bandgap semiconductors near the absorption threshold: Influence of excitonic effects," J. Quantum Electron. **32**(10), 1746–1751 (1996).
[52] C. Tanguy, "Optical dispersion by Wannier excitons," Phys. Rev. Lett. **75**, 4090 (1995).
[53] R. J. Elliott, "Intensity of optical absorption by excitons," Phys. Rev. **108**, 1384–1389 (1957).
[54] H. M. Nussenzveig, *Causality and Dispersion Relations* (Academic, New York, 1972).
[55] D. T. F. Marple, "Refractive index of GaAs," J. Appl. Phys. **35**, 1241 (1964).
[56] R. Magri, S. Froyen, and A. Zunger, "Electronic structure and density of states of the random $Al_{0.5}Ga_{0.5}As$, $GaAs_{0.5}P_{0.5}$, and $Ga_{0.5}In_{0.5}As$ semiconductor alloys," Phys. Rev. B **44**, 7947 (1991).
[57] P. Petrik, "Parameterization of the dielectric function of semiconductor nanocrystals," Physica B **453**, 2–7 (2014).
[58] B. Monemar, K. K. Shih, and G. D. Pettit, "Some optical properties of the $Al_xGa_{1-x}As$ alloys system," J. Appl. Phys. **47**, 2604 (1976).
[59] C. Bosio, J. L. Staehli, M. Guzzi, G. Burri, and R. A. Logan, "Direct-energy-gap dependence on Al concentration in $Al_xGa_{1-x}As$," Phys. Rev. B **38**, 3263 (1988).
[60] N. C. Miller, S. Zemon, G. P. Werber, and W. Powazinik, "Accurate electron probe determination of aluminum composition in (Al, Ga)As and correlation with the photoluminescence peak," J. Appl. Phys. **57**, 512 (1985).